JOURNAL OF GEOPHYSICAL RESEARCH: SPACE PHYSICS, VOL. 119, 163–170, doi:10.1002/2013JA019315, 2014

Enhanced radial transport and energization of radiation belt electrons due to drift orbit bifurcations

A. Y. Ukhorskiy,[1] M. I. Sitnov,[1] R. M. Millan,[2] B. T. Kress,[2] and D. C. Smith[1]

Received 9 September 2013; revised 11 November 2013; accepted 13 November 2013; published 8 January 2014.

[1] Relativistic electron intensities in Earth's outer radiation belt can vary by multiple orders of magnitude on the time scales ranging from minutes to days. One fundamental process contributing to dynamic variability of radiation belt intensities is the radial transport of relativistic electrons across their drift shells. In this paper we analyze the properties of three-dimensional radial transport in a global magnetic field model driven by variations in the solar wind dynamic pressure. We use a test particle approach which captures anomalous effects such as drift orbit bifurcations. We show that the bifurcations lead to an order of magnitude increase in radial transport rates and enhance the energization at large equatorial pitch angles. Even at quiet time fluctuations in dynamic pressure, radial transport at large pitch angles exhibits strong deviations from the diffusion approximation. The radial transport rates are much lower at small pitch angle values which results in a better agreement with the diffusion approximation.

Citation: Ukhorskiy, A. Y., M. I. Sitnov, R. M. Millan, B. T. Kress, and D. C. Smith (2014), Enhanced radial transport and energization of radiation belt electrons due to drift orbit bifurcations, *J. Geophys. Res. Space Physics*, *119*, 163–170, doi:10.1002/2013JA019315.

1. Introduction

[2] Relativistic electrons ($\gtrsim$ 500 keV) in the near-Earth space are organized (on average) in two populations trapped by the magnetic field and referred to as the inner and the outer radiation belts. In geomagnetically quiet conditions the belts are separated by a slot region centered at $L \sim 2.5$. During geomagnetic storms electron intensities in the outer belt can vary by orders of magnitude which some time results in transient multibelt configurations [*Baker et al.*, 2013] and particle injections into the slot region [e.g., *Baker et al.*, 2004; *Kress et al.*, 2008]. This dynamic variability is produced by a shifting balance between acceleration and loss mechanisms operating at various spatial and temporal scales [see recent reviews, *Millan and Thorne*, 2007; *Thorne*, 2010; *Millan and Baker*, 2012].

[3] One basic process underlying global variability of the radiation belts is electron transport across their drift shells, which is referred to as radial transport or radial diffusion [e.g., *Kellog*, 1959; *Tverskoy*, 1964; *Fälthammar*, 1965; *Roederer*, 1968; *Vernov et al.*, 1969; *Lyons and Thorne*, 1973]. Radial transport is commonly attributed to large-scale ultralow frequency (ULF) fluctuations of the electric and magnetic fields in the Pc4-5 frequency range (2–22 mHz) [*Jocobs et al.*, 1964]. Large-scale ULF fluctuations can exhibit resonance with the electron azimuthal drift motion. If the amplitude of ULF fluctuations is sufficiently large to produce an overlap of particle populations trapped at resonances with the adjacent harmonics of the spectrum, or alternatively, if the phase shifts across the wave spectrum vary in time, electron motion in the direction perpendicular to the drift becomes stochastic producing their scattering across the drift shells [see review, *Ukhorskiy and Sitnov*, 2012].

[4] In the dayside-compressed geomagnetic field, electron drift orbits can undergo bifurcations that abruptly violate their second adiabatic invariant and cause their scattering to high latitudes [*Northrop and Teller*, 1960; *Northrop*, 1963; *Roederer*, 1970; *Shabansky*, 1971; *Antonova et al.*, 2003; *Öztürk and Wolf*, 2007; *Kim et al.*, 2008; *Wan et al.*, 2010]. It has recently been realized [*Ukhorskiy et al.*, 2011; *Ukhorskiy and Sitnov*, 2012] that drift orbit bifurcations affect a broad region of the outer belt and can cause radial transport even in the absence of fluctuations in the field, which can enhance both energization and loss of relativistic electrons.

[5] The effects of drift orbit bifurcations were previously analyzed only in stationary magnetic field configurations, whereas most of the studies of the radial transport due to ULF waves were conducted in two-dimensional models of the equatorially mirroring electrons that do not account for the bifurcations [e.g., *Elkington et al.*, 1999, 2003; *Ukhorskiy et al.*, 2006; *Degeling et al.*, 2008; *Ukhorskiy and Sitnov*, 2008]. Here we present the first analysis of three-dimensional radial transport in global dynamic fields that

[1]Applied Physics Laboratory, Johns Hopkins University, Laurel, Maryland, USA.
[2]Dartmouth College, Hanover, New Hampshire, USA.

Corresponding author: A. Y. Ukhorskiy, Applied Physics Laboratory, Johns Hopkins University, Laurel, MD 20723 USA. (ukhorskiy@jhuapl.edu)

2169-9380/14/10.1002/2013JA019315

includes both the effects of the ULF fluctuations and drift orbit bifurcations. We examine how transport properties and energization rates are affected by drift orbit bifurcations. In the following section we discuss how to quantify radial transport across the entire outer belt including the regions affected by drift orbit bifurcations where the third adiabatic invariant is not defined. In section 3, followed by conclusions, we describe the details of our three-dimensional test particle model and present the results of our numerical simulations and their analysis.

2. Radial Transport in the Absence of L^*

[6] Relativistic electrons trapped in the geomagnetic field exhibit three-dimensional quasiperiodic motion, which consists of gyromotion around the guiding center, the bounce motion of particle guiding center along the field lines between conjugate reflection points, and gradient curvature azimuthal drift of the guiding center around Earth. Each component of the quasiperiodic motion is associated with its own adiabatic invariant. A set of three invariants defines a drift shell. Radial transport across the drift shells requires violation of the third invariant, Φ, associated with the azimuthal drift motion. In a quasi-dipole field the spatial and temporal scales of the three motions are separated by multiple orders of magnitude. Drift-resonant interaction with ULF fields, therefore, violates the third invariant without breaking either the first, μ, or the second, J, invariants.

[7] The third invariant of a radiation belt electron is the magnetic flux, which is enclosed by its unperturbed guiding center trajectory (i.e., computed in the static magnetic field fixed at a given moment of time):

$$\Phi = \oint_C \mathbf{A} \cdot \mathrm{d}\mathbf{l} = \oint_C \alpha \mathrm{d}\beta, \tag{1}$$

where $\mathbf{A}$ is the magnetic field vector potential: $\mathbf{B} = \nabla \times \mathbf{A}$, α and β are the Euler potentials [e.g., *Stern*, 1967]: $\mathbf{A} = \alpha \nabla \beta$, and the integration contour C can be chosen anywhere on the unperturbed drift bounce guiding center surface. The third invariant is often expressed in terms of the L^* variable:

$$\Phi = -\frac{2\pi B_0 R_E^2}{L^*}. \tag{2}$$

Physically, L^* is the radial distance (in Earth radii) to the equatorial points of the drift bounce shell on which the particle would be found if all nondipolar contributions to the magnetic field would be adiabatically turned off [*Roederer*, 1970]. In the above expression $B_0 \simeq 31000$ nT is the magnetic field intensity on Earth's surface at the equator, and $R_E \simeq 6380$ km is the Earth's radius. Being analogous to a dimensionless radial distance L^* is convenient for quantifying radial transport of radiation belt electrons. In particular, it allows separating transport due to violation in the third invariant, from fully adiabatic variations in radiation belt intensities in which L^* is conserved.

[8] The magnetic field, however, is not quasi-dipolar across the entire outer belt. In the outer belt regions adjacent to the magnetopause, the distribution of magnetic field intensity along the field lines, $B(s)$, has two minima below and above the equatorial plane, as opposed to the quasi-dipolar field on the nightside where $B(s)$ has a single minimum at the equator. A particle bouncing across the equator and drifting from the nightside to the dayside into the compressed field region branches off into one of the off-equatorial $B(s)$ pockets at the point where the value of $B(s)$ at the local maximum at the equator exceeds the magnetic field value at its mirror points. Such drift orbit bifurcations correspond to crossing a separatrix in the bounce phase space between trajectories across the equator and trapped at the pockets below and above the equator. As particle approaches the separatrix, its bounce period grows until in some vicinity of the separatrix the time scales of the bounce and drift motions become comparable, which breaks the adiabaticity of the bounce motion. Violation of the second invariant at bifurcations causes simultaneous scattering in the radial direction and therefore provides an additional mechanism for radial transport (for a detailed description of drift orbit bifurcations, see *Öztürk and Wolf* [2007], *Wan et al.* [2010], *Ukhorskiy et al.* [2011], and *Ukhorskiy and Sitnov* [2012]).

[9] It has been suggested [*Ukhorskiy et al.*, 2011] that drift orbit bifurcations enhance energization produced by radial transport across the outer belt. Radial transport due to only ULF waves conserves the first and the second invariants, which specifies the energy gain with inward radial transport as a unique function of the radial position. Drift orbit bifurcations break the second invariant while conserving the first invariant and the energy. The energy gain with radial transport in the presence of bifurcations, therefore, is no longer a unique function of the radial position, which can result in higher energization rates.

[10] In the bifurcation region the three-dimensional particle motion is no longer quasiperiodic. Unperturbed (i.e., in a static magnetic field) drift bounce orbits do not conserve the second invariant, and the third adiabatic invariant therefore is undefined. To quantify radial transport across the entire belt including the bifurcation region, we generalize definition (1) of the third invariant by changing the integration from the unperturbed drift shells to the actual drift bounce orbits in time-varying magnetic field:

$$\bar{\Phi} = \int_0^{2\pi} \alpha \mathrm{d}\beta = -\frac{2\pi B_0 R_E^2}{\bar{L}}. \tag{3}$$

The generalized $\bar{L}$ variable is expected to be a good measure of radial transport because (a) for quasiperiodic orbits in a static field, $L^* = \bar{L}$; (b) for time-varying adiabatic variations in the field ($\Phi = \text{const}$), $L^* \simeq \bar{L}$; (c) for non-adiabatic transport ($\Phi \neq \text{const}$), $\bar{L}$ is approximately the average of L^* over particle drift orbits.

3. Test Particle Simulations

[11] To simulate the global distribution and large-scale variability of magnetic field across the outer belt, we used the [*Tsyganenko and Stern*, 1996] (T96) magnetic field model. Time dependence in the model comes from varying solar wind and geomagnetic input parameters. The inductive electric field induced by the magnetic field variations was calculated as the time derivative of the magnetic field vector potential: $\mathbf{A} = \alpha \nabla \beta$. The Euler potentials α and β were computed by tracing magnetic field lines to Earth's surface, where their values were determined from the analytical

expressions for a dipole magnetic field similarly to [*Fok and Moore*, 1997]

$$\alpha = -B_0 \frac{\sin^2\theta}{r};\ \beta = \varphi, \tag{4}$$

where (r, θ, φ) are the spherical coordinates of the foot points of the traced field lines.

[12] As was previously shown [*Ukhorskiy and Sitnov*, 2008], fluctuations of the magnetic and inductive electric fields in the model induced by variations in the solar wind dynamic pressure have properties of $m = 1$ ULF waves observed in the inner magnetosphere and therefore provide a good proxy of large-scale ULF activity that drives radial transport across the outer belt.

[13] In this study the T96 model was driven with the dynamic pressure time series corresponding to quiet time solar wind conditions and generated as

$$P_{\mathrm{dyn}}(t) = P_0 + \Delta P \sum_{k=1}^{N} k^{-\beta/2} \sin(k\Delta\omega t + \psi_k), \tag{5}$$

with $P_0 = 4$ nPa. The spectral exponent $\beta = 5/3$, the number of harmonics $N = 50$, the spectral density $\Delta\omega = 2\pi \cdot 0.1$ mHz, and the random phase shifts between spectral harmonics $\psi_k \in (0, 2\pi]$ were chosen similarly to *Ukhorskiy and Sitnov* [2008]. The amplitude value ΔP was selected such that the root-mean-square amplitude of pressure variations was $P^{\mathrm{rms}} = 0.6$ nPa. All other T96 input parameters remained fixed at quiet time values: $Dst = 0$, IMF $B_z = 5$ nT, and IMF $B_y = 0$.

[14] Radial transport was then simulated in three dimensions with the use of large ensembles of test particles. Particle motion was calculated in the guiding center approximation based on our Hamiltonian formulation [*Ukhorskiy et al.*, 2011]:

$$\begin{cases} \dfrac{d\mathbf{R}}{dt} = \dfrac{p_\parallel}{m\gamma}\dfrac{\mathbf{B}^*}{B_\parallel^*} + c\dfrac{\mathbf{E}^* \times \hat{\mathbf{b}}}{B_\parallel^*} \\ \dfrac{dp_\parallel}{dt} = e\dfrac{\mathbf{E}^* \cdot \mathbf{B}^*}{B_\parallel^*} \\ \mu = \dfrac{p_\perp^2}{2mB} = \mathrm{const} \end{cases}, \tag{6}$$

where $\mathbf{R}$ is the guiding center position, $p_\parallel$ and $p_\perp$ are the momentum components parallel and perpendicular to the field lines, $\hat{\mathbf{b}}$ is the unitary vector parallel to the magnetic field, e and m are the electron charge and mass, γ is the relativistic factor, and the effective fields $\mathbf{E}^*$ and $\mathbf{B}^*$ are defined in terms of the effective potentials:

$$\begin{aligned} &\mathbf{B}^* = \nabla \times \mathbf{A}^*;\ \mathbf{E}^* = -\nabla\Phi^* - \frac{1}{c}\frac{\partial \mathbf{A}^*}{\partial t} \\ &\mathbf{A}^* = \mathbf{A} + \frac{c}{e}p_\parallel \hat{\mathbf{b}};\ e\Phi^* = mc^2\gamma \end{aligned}. \tag{7}$$

[15] To investigate how drift orbit bifurcations affect radial transport and energization, we compare the results of two simulations with small and large initial values of the second invariant. At large values of the second invariant, corresponding to small equatorial pitch angles, particles are not susceptible to bifurcations and radial transport in this case is attributed solely to drift-resonant interaction with pressure-induced ULF fluctuations in the field, whereas the radial transport of particles at small values of the second invariant, corresponding to near-equatorial (i.e., with mirror points close to the equator) particles, is driven by a combination of the ULF fluctuations and drift orbit bifurcations.

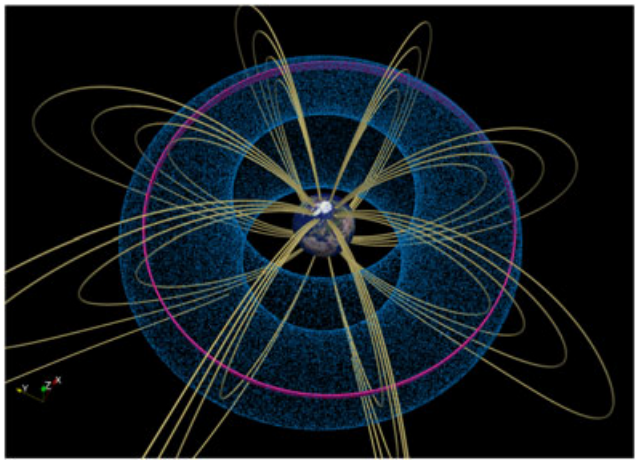

Figure 1. Unperturbed electron drift shells at $P_{\mathrm{dyn}} = 4$ nPa and zero dipole tilt angle used to initialize test particle simulations of radial transport. The drift shell correspond to $\bar{L} = 5.5$, $L_M = 5.5$ and $\alpha_{\mathrm{eq}} = 85°$ (red) and $\bar{L} = 5.7$, $L_M = 6.5$ and $\alpha_{\mathrm{eq}} = 15°$ (blue) at midnight.

[16] Electrons were initiated on two stable unperturbed drift shells at $P_{\mathrm{dyn}} = 4$ nPa with similar values of $\bar{L}$. The two initial drift shells are separated at midnight and closely approach at noon (Figure 1). The large pitch angle shell corresponds to $\bar{L} = 5.5$ and the equatorial radial distance and pitch angles at midnight of $L_M = 5.5$ and $\alpha_{\mathrm{eq}} = 85°$, while the small pitch angle shell corresponds to $\bar{L} = 5.7$, $L_M = 6.5$, and $\alpha_{\mathrm{eq}} = 15°$. In both simulations, we used ensembles of 10^5 electrons with the relativistic factor $\gamma = 3$ (~ 1 MeV) evenly distributed in the drift and bounce phases along the initial drift shells.

[17] Electron transport in the case of near-equatorial particles is illustrated in Figure 2 which shows four snapshots of transport during different times of the simulation process. Figure 2 (top row) shows electron positions projected along the field lines onto the equatorial plane. Figure 2 (middle row) shows the second adiabatic invariant. In Figure 2 (top and middle rows), particle energy is marked with color. Figure 2 (bottom row) shows radial distribution function $f(\bar{L})$ defined as the number of particles between $\bar{L}$ and $\bar{L}+d\bar{L}$. Figure 2 (first column) show initial conditions. Figure 2 (second column) corresponds to 0.55 h after the simulation start. A single fold formed in the ring of particles at noon (Figure 2, top row) is indicative of resonant interaction of the electron drift motion with the pressure-induced ULF fluctuations of the azimuthal electric field [*Ukhorskiy and Sitnov*, 2008, 2012; *Kress et al.*, 2012].

[18] After about 2.3 h into the simulation process, the electron population expanded into the drift bifurcation region. The effects of bifurcations can be seen in Figure 2 (third column) which illustrates the state of the system at 2.95 h shortly after the bifurcation onset. Particles on the bifurcated orbits bouncing above or below the equatorial plane are indicated with purple in the Figure 2 (top row). Figure 2 (middle row) shows the spread in the second invariant at high L shells due to bifurcations.

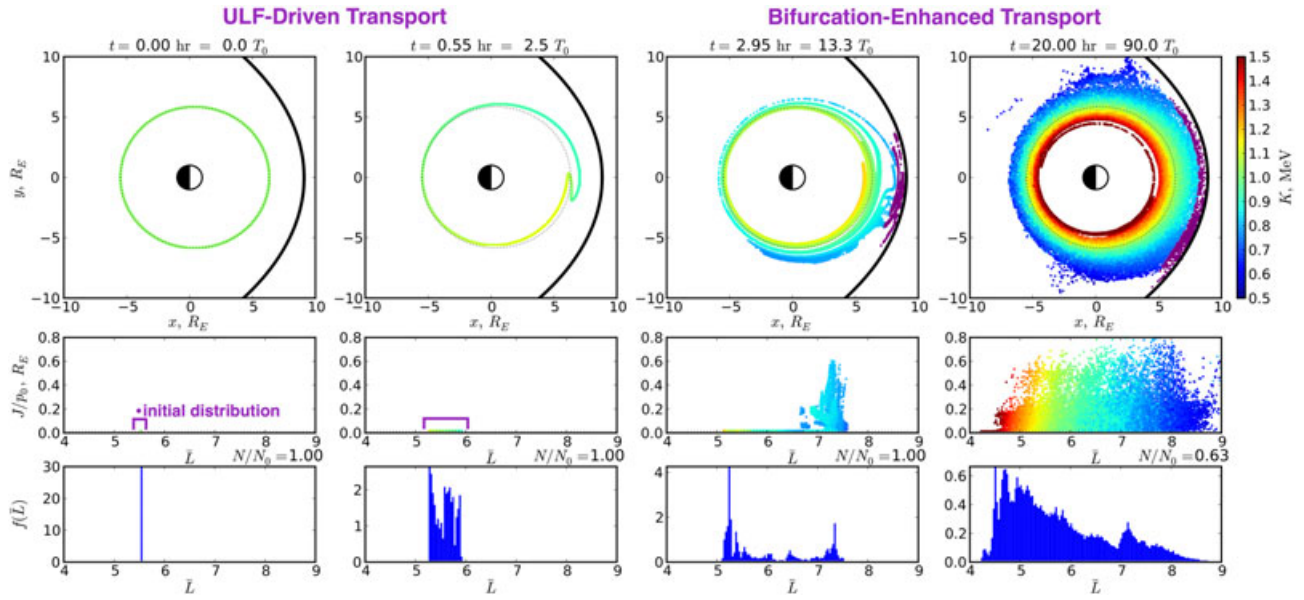

Figure 2. Three-dimensional test particle simulation of 10^5 near-equatorial electrons with the initial energy of 1 MeV in the magnetic field with large-scale ULF fluctuations induced by the solar wind dynamic pressure. (top row) Instantaneous equatorial projection (along the magnetic field lines) of electron position. Particle energy is marked with color. Electrons on the bifurcating orbits bouncing either below or above the equator are marked with purple. (middle row) The second adiabatic invariant. (bottom row) The radial distribution function.

[19] After 20 h by the end of the simulation (Figure 2, fourth column), the inner edge of the particle population reached down to $\bar{L} \sim 4$ and about 40% of particles were lost from the belt through the magnetopause. Figure 2 (middle row) shows that the spread in the second invariant expanded over almost the entire range of drift shells populated by particles and not just the outer range directly affected by the bifurcations. This indicates that some particles after bifurcations were radially transported inward due to resonant interaction with ULF fluctuations.

3.1. Radial Transport Rates and Properties

[20] Our initial test particle distributions correspond to delta function initial conditions on the particle distribution function in the invariant space: $f(J, \bar{L}, t = 0) = \delta(J - J_0)\delta(\bar{L} - \bar{L}_0)$. Test particle trajectories therefore provide a numerical estimate of the Green's function of the underlying transport equation. If radial transport in the system obeys a Fokker-Plank equation, then (in some vicinity of the initial $\bar{L}_0$) the second moment of the distribution function scales linearly with time:

$$\langle(\Delta\bar{L}(t))^2\rangle = \langle(L(t) - \langle\bar{L}\rangle)^2\rangle = 2D_{\bar{L}\bar{L}}(J, \bar{L}_0)t, \qquad (8)$$

where $D_{\bar{L}\bar{L}}$ is the local value of the diffusion coefficient and $\langle\cdots\rangle$ denotes averaging over the ensemble of particles.

[21] Radial transport rates during first 8 h of the simulation with a small initial value of the second invariant are shown in Figure 3a. Red line corresponds to $\langle(\Delta\bar{L})^2\rangle$ computed over the entire ensemble, while black lines show $(\Delta\bar{L})^2$ of 80 sample trajectories. Variation of the second adiabatic invariant across the ensemble is illustrated in Figure 3c. The average value of the second invariant is shown with red. The black lines correspond to the invariant values of 80 sample trajectories, same as shown in Figure 3a. The second invariant is conserved until the onset of drift orbit bifurcations at 2.3 h. At bifurcations, the second invariant exhibits jumps and is approximately conserved between bifurcations.

[22] It is evident from Figure 3a that the radial transport rates rapidly increase at the bifurcation onset: there is approximately a factor of 10 increase in the average slope of $\langle(\Delta\bar{L})^2\rangle$, which is maintained till the onset of the magnetopause losses at 5.3 h. The subsequent large variations in $\langle(\Delta\bar{L})^2\rangle$ are mostly cased by the change in the magnetopause location and the loss of particles from the outermost drift shells.

[23] From Figure 3a, it follows that $\langle(\Delta\bar{L})^2\rangle$ does not increase with time monotonically prior to the onset of magnetopause losses. This means that the radial transport cannot be approximated by a Fokker-Plank equation. This is attributed to the fact that the drift-phase correlations among particles in the ensemble do not fully decay by the time it takes the ensemble to expand over the entire system (i.e., reach the magnetopause). The persistence of phase correlations is also manifested in filamentary multipeak structure of radial distribution function $f(\bar{L})$ maintained throughout the entire simulation (Figure 2, bottom row). Consequently, particle distribution function cannot be averaged over the drift phase in the spirit of the Fokker-Plank equation (for more discussion, see *Ukhorskiy et al.* [2006], *Ukhorskiy and Sitnov* [2008, 2012], and *Kress et al.* [2012]).

[24] Radial transport of particles with small equatorial pitch angles not susceptible to drift orbit bifurcations is shown in Figure 4. Figure 4a shows the transport over the entire simulation. It is evident that the transport rates are much slower than in the previously considered case of the

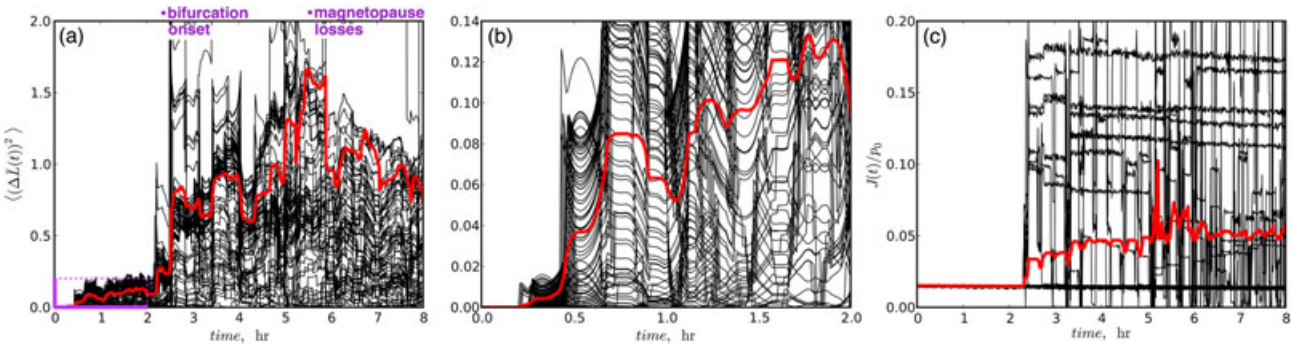

Figure 3. (a, b) Radial transport and the second adiabatic invariant in test particle simulations of the near-equatorial particles (L_M = 5.5, α_{eq} = 85°). Black lines show time variation of $\bar{L}^2$ and J/p_0 of 80 sample trajectories from the simulation, while red lines correspond to average values computed with all trajectories. Figure 3a shows the transport during the entire simulation, while Figure 3b zooms in on the first 2 h.

near-equatorial particles. Over 20 h, particles with small equatorial pitch angles expanded only over a small fraction of the outer belt, which was covered by the near-equatorial particles over less than 1.5 h. Since the transport is much slower, the drift-phase correlations among particles of the ensemble decay well before the particles expand over the entire system. Consequently, radial transport on the time scales of $\gtrsim$ 20 h is in a much better agreement with radial diffusion, which is evident in nearly linear scaling of $\langle(\Delta\bar{L})^2\rangle$ in Figure 4a.

[25] Similarly to Figure 3a, Figure 4b shows the transport during first 8 h of the simulation. According to the figure non-monotonic variations of $\langle(\Delta\bar{L})^2\rangle$ become more prominent on this time scales. Consequently, even at small equatorial pitch angles the radial transport cannot be well approximated with a Fokker-Plank equation on the timescales of $\lesssim$ 10 h.

[26] Figures 3b and 4c show the comparison of radial transport of near-equatorial and small pitch angle particles during first 2 h prior to the onset of drift orbit bifurcations in the case of near-equatorial particles. It is therefore expected that over this time period, radial transport in both cases is attributed to only resonant interaction of the electron drift motion with the ULF fluctuations induced by variations in the solar wind dynamics pressure. Since the initial $\bar{L}$ values were similar in both cases, an order of magnitude difference in the transport rates must be explained by the difference in the ULF power along the drift bounce orbits of particles at different equatorial pitch angles.

[27] We examine the pitch angle dependence of the ULF-driven radial transport rates analytically in a dipole magnetic field, which is a reasonable approximation in the regions far from drift obit bifurcations. Transport across the drift shells is attributed to the radial $\mathbf{E} \times \mathbf{B}$ drift due to the azimuthal electric field of the ULF fluctuations: $u_r = cE_\varphi/B$. The drift velocity varies over the particle bounce period. The radial displacement over a bounce period is given by the integral of u_r. Since the bounce period depends on the equatorial pitch angles, to assess the difference in transport rates at different pitch angles, one must compare the radial displacements per unit time, which is given by the bounce-averaged drift velocity:

$$\bar{u}_r = \frac{4c}{T_b(\alpha_{eq})} \int_0^{T_b/4} \frac{E_\varphi}{B} \mathrm{d}t, \tag{9}$$

where T_b is the bounce period.

[28] The estimate of the bounce-averaged drift velocity is described in Appendix A. According to equation (A10), a decrease of the equatorial pitch angle from 90° to 55° leads to a factor of two decrease in the radial transport rate. The

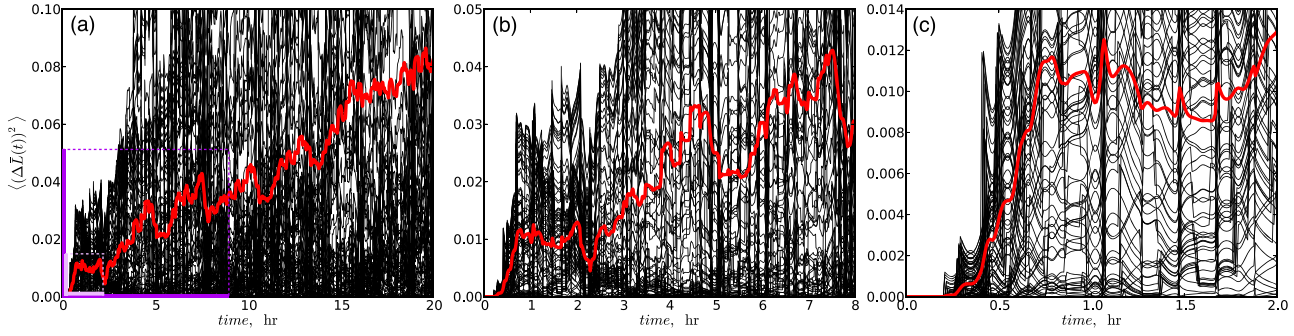

Figure 4. Radial transport in test particle simulations of electrons with small equatorial pitch angles (L_M = 6.5, α_{eq} = 15°). Similar to Figure 3, black lines show 80 sample trajectories, while red lines correspond to average values computed with all trajectories in the simulation. Figure 4a shows the transport during the entire simulation, while Figures 4b and 4c zoom in on the first 8 and 2 h correspondingly.

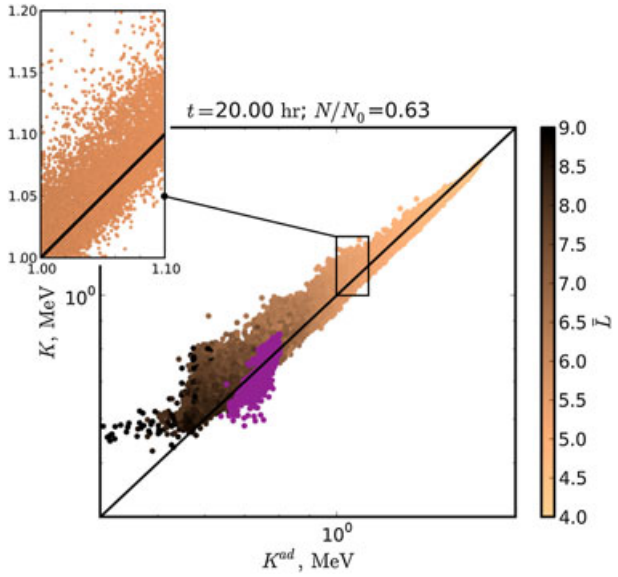

Figure 5. The comparison of the energy K of the near-equatorial electrons after 20 h of radial transport enhanced by drift orbit bifurcations, which conserve the first but violate the second invariant; with the energy K^{ad}, the electrons would have had if the transport conserved both the first and the second invariants. Electron radial position $\bar{L}$ is marked with color. Electrons on the bifurcating orbits bouncing either below or above the equator are marked with purple.

ratio of transport rates at equatorial pitch angles of 15° and 85° used in our simulations is approximately

$$\frac{\langle(\Delta\bar{L}(15°))^2\rangle}{\langle(\Delta\bar{L}(85°))^2\rangle} \simeq \frac{\bar{u}_r(15°)^2}{\bar{u}_r(85°)^2} \simeq 0.1, \tag{10}$$

which is in a good agreement with the simulation results.

3.2. Electron Energization

[29] If radial transport conserves both the first and the second invariants, as in the case of transport due to drift-resonant interactions with ULF fields, the particle energy is a function of the radial position $\bar{L}$ and the initial value of the equatorial pitch angle, which specifies the second invariant. Thus, in a dipole magnetic field, the L dependence of electron momentum p varies between L^{-1} and $L^{-3/2}$ depending on the value of the second invariant [e.g., *Schulz and Lanzerotti*, 1974].

[30] It has been suggested [e.g., *Ukhorskiy et al.*, 2011] that drift orbit bifurcations can enhance the level of energization produced by radial transport. Consider a near-equatorial particle ($J \simeq 0$) initially at $\bar{L}_0$. Bifurcations violate the second adiabatic invariant without changing particle energy. After a bifurcation on the dayside, its second invariant will increase, which will require a decrease in the perpendicular energy. To conserve the first adiabatic invariant, $\mu = p_\perp^2/2B$, the particle will move outward to $\bar{L}_1$ where the magnetic field is weaker. Thus, if the particle is then transported inward to some $\bar{L}_2 < \bar{L}_0$ due to drift-resonant interaction with ULF fluctuations, it will acquire more perpendicular energy then a particle transported from $\bar{L}_0$ to $\bar{L}_2$ directly without a drift orbit bifurcation.

[31] To address the effect of drift orbit bifurcations on electron energization during radial transport, we compare the distribution of particle energy K at the end of our simulation of the near-equatorial particles with the energy K^{ad} that the particles would have had if the transport conserved both the first and the second invariants. Since initially the second invariant in this simulation was approximately zero, the energy of adiabatic transport was estimated from the conservation of the first invariant: $K^{ad} = m_e c^2(\gamma^{ad} - 1)$, $\gamma^{ad} = \sqrt{2\mu B/m_e c^2 + 1}$. The results are shown in Figure 5. Particle radial position $\bar{L}$ is indicated with color. Electrons on bifurcating orbits bouncing either above or below the equator are marked with purple. Transport that conserves both invariants is constrained to the line $K = K^{ad}$. The vertical spread of particle energy across this line is caused by drift orbit bifurcations. The energy spread is larger ($\sim$ 60%) at lower energies corresponding to large $\bar{L}$ values close to the bifurcation region. The narrowing of the energy spread with increase in energy is attributed to the diminishing of radial transport rates with decrease in $\bar{L}$, which makes it more probable for a particle to escape from the magnetopause than to be transported to low $\bar{L}$. Nonetheless, some of the particles at 1 MeV have energies 20% higher than what they would have acquired with transport without drift orbit bifurcations.

4. Conclusions

[32] In this paper, we investigated the properties of three-dimensional radial transport in the outer radiation belt, including the effects of drift orbit bifurcations. For this purpose, we used test particle simulations in the guiding center approximations. Radial transport was driven by resonant interaction of the electron drift bounce motion with large-scale ULF fluctuations in the magnetic field induced by variations in the solar wind dynamic pressure.

[33] In the absence of bifurcations (i.e., at constant first and second adiabatic invariants), radial transport rates exhibit strong dependence on the equatorial pitch angle. Transport rates decrease by a factor of 2 if the pitch angle is decreased from 90° to 55° and by a factor of 10 if the pitch angle is further decreased to 15°. Even at low fluctuations in dynamic pressure considered in this paper, radial transport rates at large pitch angles is sufficiently large for an ensemble of particles initiated at a single L shell to expand over the entire outer belt before the drift-phase correlations among the particles have time to decay. Consequently, radial transport at large pitch angles exhibits large deviations for the radial diffusion approximations. Due to much lower transport rates, the dynamics of particles with small pitch angles become independent of their initial drift-phase distribution well before they expand over the entire system and their radial transport at long time scales ($\gtrsim$ 20 h) attain an approximate agreement with radial diffusion.

[34] Radial transport of radiation belt electrons at large pitch angles is affected by drift orbit bifurcations. It was shown that bifurcations lead to an order of magnitude increase in radial transport rates. Drift orbit bifurcations conserve the first adiabatic invariant but violate the second adiabatic invariant. The radial transport in the presence of bifurcations can produce a stronger energization of radiation belt particle than a transport that conserves both the

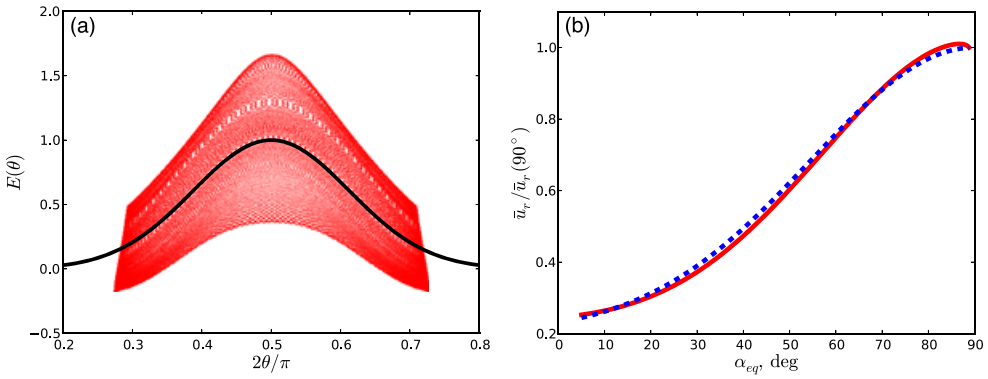

Figure A1. Panel (a): Latitudinal profiles of the ULF fluctuations in the T96 model computed at different values of the magnetic local time (red) and the Gaussian fit (black) used for their approximation in the computation of radial transport rates. Panel (b): A numerical estimate (red) and an analytical approximation (blue) of the bounce-averaged velocity of radial $\mathbf{E} \times \mathbf{B}$ drift as function of the equatorial pitch angle.

first and the second adiabatic invariants. While the effect is most prominent at lower energies and high L shells, a 20% increase of energization was observed at 1 MeV in the center of the outer belt at $\bar{L} = 5.5$.

Appendix A: Pitch Angle Dependence of Radial Transport Rates

[35] The rate of radial transport of electrons at a given value α_{eq} of the equatorial pitch angle due to ULF fluctuations in electric field can be estimated from the bounce-averaged value of the radial component of the $\mathbf{E} \times \mathbf{B}$ drift velocity:

$$\bar{u}_r = \frac{4c}{T_b(\alpha_{eq})} \int_0^{T_b/4} \frac{E_\varphi}{B} \mathrm{d}t, \tag{A1}$$

where T_b is the bounce period. The azimuthal electric field of the ULF fluctuations can be represented as $E_\varphi = E(\varphi, t)E(\theta)$, where $E(\varphi, t)$ is the azimuthal distribution of the field intensity which varies on the ULF time scales and therefore can be considered stationary on the time scales of the bounce motion, and $E(\theta)$ is the latitudinal dependence of the field intensity.

[36] The bounce period can be estimated as [*Hamlin et al.*, 1961]

$$T_B = \frac{4LR_E}{v} \tau(\alpha_{eq}), \tag{A2}$$

where

$$\tau(\alpha_{eq}) = 1.38 - 0.32(\sin\alpha_{eq} + \sin^2\alpha_{eq}). \tag{A3}$$

[37] After using the following substitutions,

$$dt = ds/v\cos\alpha(\theta, \alpha_{eq}), \tag{A4}$$

$$ds = LR_E \sin\theta\sqrt{1 + 3\cos^2\theta}, \tag{A5}$$

$$B(L, \theta) = B(L)\frac{\sqrt{1 + 3\cos^2\theta}}{\sin^6\theta} \tag{A6}$$

we obtain

$$\bar{u}_r = \frac{u_E(L)}{\tau(\alpha_{eq})} \int_0^{\theta_m} \frac{E(\theta)\sin^7\theta}{\cos\alpha(\theta, \alpha_{eq})} \mathrm{d}\theta, \tag{A7}$$

where $u_E = cE(\varphi, t)/B(L)$ is the equatorial $\mathbf{E}\times\mathbf{B}$ drift velocity.

[38] The latitudinal dependence of $\cos\alpha$ can be expressed as

$$\cos\alpha = \left(1 - \sin^2\alpha_{eq}\frac{\sqrt{1 + 3\cos^2\theta}}{\sin^6\theta}\right)^{1/2}. \tag{A8}$$

To approximate the latitudinal distribution of the ULF fluctuations, we used the Gaussian function

$$E(\theta) = \exp\left[-\left(\frac{\theta - \pi/2}{\Delta\theta}\right)^2\right], \tag{A9}$$

which was fitted into the latitudinal profiles of the electric field fluctuations in our model, computed at different values of the magnetic local time (Figure A1a) to determine $\Delta\theta = 0.5$.

[39] After inserting expression (A9) into (A7) and computing the integral numerically for different values of α_{eq}, it was found that the bounce-averaged velocity of the electron radial drift depends on the equatorial pitch angle as approximately

$$\bar{u}_r = u_E(L)\left\{a + b\exp\left[-\left(\frac{\alpha_{eq} - \pi/2}{\Delta\alpha}\right)^2\right]\right\}, \tag{A10}$$

where $a = 0.20$, $b = 0.80$, and $\Delta\alpha = 0.87$ (Figure A1b).

[40] **Acknowledgments.** The research was supported by NSF grant AGS1059736, NASA grant NNX11AO74G, and NASA contract NAS5-01072 through a subcontract from NJIT 999640 - I.

[41] Masaki Fujimoto thanks the reviewers for their assistance in evaluating this paper.

References

Antonova, A. E., Y. I. Gubar', and A. P. Kropotkin (2003), Effects in the radiation belts caused by the second adiabatic invariant violation in the presence of dayside off-equatorial magnetic field minima, *Adv. Space Res.*, *31*, 1223–1228.

Baker, D. N., S. G. Kanekal, X. Li, S. P. Monk, J. Goldstein, and J. L. Burch (2004), An extreme distortion of the Van Allen belt arising from the 'Hallowe'en' solar storm in 2003, *Nature*, *432*, 878–881.

Baker, D. N., et al. (2013), A long-lived relativistic electron storage ring embedded in Earth's outer Van Allen belt, *Nature*, *340*, 186–190, doi:10.1126/science.1233518.

Degeling, A. W., L. G. Ozeke, R. Rankin, I. R. Mann, and K. Kabin (2008), Drift resonant generation of peaked relativistic electron distributions by Pc 5 ULF waves, *J. Geophys. Res.*, *113*, A02208, doi:10.1029/2007JA012411.

Elkington, S. R., M. K. Hudson, and A. A. Chan (1999), Acceleration of relativistic electrons via drift-resonant interaction with toroidal-mode Pc-5 ULF oscillations, *Geophys. Res. Lett.*, *26*, 3273–3276.

Elkington, S. R., M. K. Hudson, and A. A. Chan (2003), Resonant acceleration and diffusion of outer zone electrons in an asymmetric geomagnetic field, *J. Geophys. Res.*, *108*(A3), 1116, doi:10.1029/2001JA009202.

Fälthammar, C.-G. (1965), Effects of time-dependent electric fields on geomagnetically trapped radiation, *J. Geophys. Res.*, *70*, 2503–2516.

Fok, M.-C., and T. E. Moore (1997), Ring current modeling in a realistic magnetic field configuration, *Geophys. Res. Lett.*, *24*, 1775–1778.

Hamlin, D. A., R. Karplus, R. C. Vik, and K. M. Watson (1961), Mirror and azimuthal drift frequencies for geomagnetically trapped particles, *J. Geophys. Res.*, *66*, 1–4.

Jocobs, J. A., Y. Kato, S. Matsushita, and V. A. Troitskaya (1964), Classification of geomagnetic micropulsations, *J. Geophys. Res.*, *69*, 180–181.

Kellog, P. J. (1959), Van Allen radiation of solar origin, *Nature*, *183*, 1295–1297.

Kim, K. C., D.-Y. Lee, H.-J. Kim, L. R. Lyons, E. S. Lee, M. K. Öztürk, and C. R. Choi (2008), Numerical calculations of relativistic electron drift loss effect, *J. Geophys. Res.*, *113*, A09212, doi:10.1029/2007JA013011.

Kress, B. T., M. K. Hudson, M. D. Looper, J. G. Lyon, and C. C. Goodrich (2008), Global MHD test particle simulations of solar energetic electron trapping in the Earth's radiation belts, *J. Atmos. Sol. Terr. Phys.*, *70*, 1727–1737.

Kress, B. T., M. K. Hudson, A. Y. Ukhorskiy, and H.-R. Mueller (2012), Nonlinear radial transport in the Earth's radiation belts, in *Dynamics of the Earth's Radiation Belts and Inner Magnetosphere, Geophys. Monogr. Ser.,* vol. 199, edited by D. Summers et al., pp. 151–160, AGU, Washington, D. C., doi:10.1029/2012GM001333.

Lyons, L. R., and R. M. Thorne (1973), Equilibrium structure of radiation belt electrons, *J. Geophys. Res.*, *78*, 2142–2149.

Millan, R. M., and D. N. Baker (2012), Acceleration of particles to high energies in Earth's radiation belts, *Space Sci. Rev.*, *173*, 103–131, doi:10.1007/s11214-012-9941-x.

Millan, R. M., and R. M. Thorne (2007), Review of radiation belt relativistic electron losses, *J. Atmos. Sol. Terr. Phys.*, *69*, 362–377.

Northrop, T. G. (1963), *The Adiabatic Motion of Charged Particles*, Interscience, New York.

Northrop, T. G., and E. Teller (1960), Stability of the adiabatic motion of charaged particles in the Earth's field, *Phys. Rev.*, *117*, 215–225.

Öztürk, M. K., and R. A. Wolf (2007), Bifurcation of drift shells near the dayside magnetopause, *J. Geophys. Res.*, *112*, A07207, doi:10.1029/2006JA012102.

Roederer, J. G. (1968), Experimental evidence on radial diffusion of geomagnetically trapped particles, in *Earth's Particles and Fields*, edited by B. M. McCormac, 143 pp., Reinhold, New York.

Roederer, J. G. (1970), Dynamics of geomagnetically trapped radiation, in *Physics and Chamestry in Space,* vol. 2, edited by J. G. Roederer and J. Zahringer, Springer-Verlag, Berlin, Heidelberg, New York.

Schulz, M., and L. J. Lanzerotti (1974), *Particle Diffusion in the Radiation Belts, Physics and Chemistry in Space,* vol. 7, Springer-Verlag, Berlin, Heidelberg, New York.

Shabansky, V. P. (1971), Some processes in the magnetosphere, *Space Sci. Rev.*, *12*(3), 299–418.

Stern, D. (1967), Geomagnetic Euler potentials, *J. Geophys. Res.*, *72*, 3995–4005.

Thorne, R. M. (2010), Radiation belt dynamics: The importance of wave-particle interactions, *Geophys. Res. Lett.*, *37*, L22107, doi:10.1029/2010GL044990.

Tsyganenko, N. A., and D. P. Stern (1996), Modeling the global magnetic field of the large-scale Birkeland current systems, *J. Geophys. Res.*, *101*, 27,187–27,198.

Tverskoy, B. A. (1964), Dynamics of the radiation belts of the Earth, 2, *Geomagnetizm and Aeronomy*, *4*, 436.

Ukhorskiy, A. Y., and M. I. Sitnov (2008), Radial transport in the outer radiation belt due to global magnetospheric compressions, *J. Atmos. Sol. Terr. Phys.*, *70*, 1714–1726.

Ukhorskiy, A. Y., and M. I. Sitnov (2012), Dynamics of radiation belt particles, *Space Sci. Rev.*, *179*, 545–578, doi:10.1007/s11214-012-9938-5.

Ukhorskiy, A. Y., B. J. Anderson, K. Takahashi, and N. A. Tsyganenko (2006), The impact of ULF oscillations in solar wind dynamic pressure on the outer radiation belt electrons, *Geophys. Res. Lett.*, *33*, L06111, doi:10.1029/2005GL024380.

Ukhorskiy, A. Y., M. I. Sitnov, R. M. Millan, and B. T. Kress (2011), The role of drift orbit bifurcations in energization and loss of electrons in the outer radiation belt, *J. Geophys. Res.*, *116*, A09208, doi:10.1029/2011JA016623.

Vernov, S. N., E. V. Gorchakov, S. N. Kuznetsov, Y. I. Logachev, E. N. Sosnovets, and V. G. Stolpovsky (1969), Particle fluxes in the outer geomagnetic field, *Rev. Geophys.*, *7*, 257–280.

Wan, Y., S. Sazykin, R. A. Wolf, and M. K. Öztürk (2010), Drift shell bifurcation near the dayside magnetopause in realistic magnetospheric magnetic fields, *J. Geophys. Res.*, *115*, A10205, doi:10.1029/2010JA015395.